Mechanism of endosomal escape by *p*H-responsive nucleic-acid vectors

Shih-Min Chang, Chia Ying Yu, and Yi-Fan Chen*
Department of Chemical and Materials Engineering, National Central University, Taoyuan 32001, Taiwan

(Received 12 April 2022; accepted 8 August 2022; published 28 September 2022)

Successful intracellular delivery of nucleic acids (NAs) hinges on many factors, one of them being NAs' efficacious escape from endosomes. As competent NA vectors, *p*H-responsive gemini surfactants (GSs) might achieve high efficacy by facilitating endosomal escape. However, how the GSs assist the escape remains debated as many proposed mechanisms still lack experimental support, which hinders replication and further improvement of the efficient delivery. Here, via UV, fluorescence spectroscopy, and small-angle neutron scattering (SANS), we examined a *p*H-responsive GS's and a *p*H-unresponsive GS's capabilities to compact DNA and withstand binding competition, and their interactions with model endosomal and lysosomal membranes, at varied *p*Hs. Acidification-driven enhancement of DNA-compaction capability and of stability against binding competition were found specific to the *p*H-responsive GS. Alongside the *p*H-responsive GS's structural perturbation to the membranes as observed with SANS, the features suggest that *p*H-responsive GSs facilitate endosomal escape by releasing excess GS molecules from DNA-GS complexes upon acidification in endosome maturation, with the released GS molecules disrupting endosomal and lysosomal membranes and thereby assisting the escape. A general design principle for NA vectors is proposed on the basis of this experimental finding.

DOI: 10.1103/PhysRevE.106.034408

I. INTRODUCTION

Intracellular delivery of nucleic acids (NAs) is of great therapeutic value. It has long been a promising, and in some cases proven, means to treat diseases involving faulty genes [1,2]; with the advent of the CRISPR-Cas9 techniques, co-delivery of single-guide RNA and the mRNA encoding Cas9 proteins has opened up an avenue for precision gene editing [3,4]. In this pandemic era, intracellular delivery of NA has become even more relevant: COVID-19 vaccines based on intracellular delivery of mRNA encoding the spike proteins of SARS-CoV-2 have been lifting the world from the pandemic-imposed lockdowns [5]. To intracellularly deliver NAs, one of the first and foremost tasks is to compact spatially extended NA coils into tightly packed globules [6,7], just like the need to compact DNA with histone proteins to package them in nuclei. This requirement is often fulfilled with NA vectors, which also protect NAs from enzymatic degradation and facilitate their delivery.

NA vectors can be classified into viral and nonviral vectors. While safer and more versatile than their viral counterparts, nonviral vectors suffer from low delivery efficacy [8]. Hence, research efforts have been committed to improving the efficacy of nonviral vectors, and many new classes of NA vectors were introduced. Among them are gemini surfactants (GSs). GSs differ from conventional surfactants by their dimerlike chemical structures. They are not unlike two molecules of conventional surfactants combined into a single one via the link of a spacer. The spacers provide an extra layer of chemical flexibility for tuning the surfactants. While GSs have displayed superior DNA delivery efficacy than conventional surfactants, functionalizing the spacers with *p*H-responsive groups improves the efficacy even further, beyond the efficacy of the benchmark, lipofectamines [9,10]. The improvement arising from the *p*H responsiveness is also observed for other classes of NA vectors, including copolymers [11], peptides [12], and lipids [13]. Facilitating endosomal escape by the vectors is considered as a reason behind this improvement [14,15]. With endocytosis being the major pathway for NA intracellular delivery [16,17], facilitating the escape from endosomes and lysosomes of NA-vector complexes is of paramount importance since entrapment in endosomes and lysosomes means demise to the complexes due to the enzymatic degradation in lysosomes.

Several mechanisms were proposed to account for the enhanced endosomal escape by *p*H-responsive vectors, with the *proton sponge* being the leading one [14]. In this mechanism, *p*H-responsive vectors are envisioned to behave as buffers and become protonated upon acidification when endocytosis progresses from the extracellular stage ($p\mathrm{H} = 7.4$), through the early ($p\mathrm{H} = 6$) and late ($p\mathrm{H} = 5$) endosome stages, to the lysosome stage ($p\mathrm{H} = 4.5$) [18]. To achieve the required acidity, the proton pumps in endosomal membranes would keep pumping protons into endosomes and lysosomes, alongside chloride counterions, when the buffering effect of the vectors takes place. The excessive chloride influx creates osmotic pressures across endosomal membranes and eventually ruptures them, allowing the complexes to escape from endosomes and lysosomes. This mechanism was also invoked to explain the high transfection efficacy of *p*H-responsive GSs [10], though without direct experimental evidence to support the claim. In fact, despite being widely accepted, the proton sponge is countered by

*yifanchen@ncu.edu.tw

many conflicting experimental observations [19–21], casting serious doubt on the validity of the mechanism. Hence, exploring the mechanisms that are actually responsible for the high efficacy of *p*H-responsive GSs, and *p*H-responsive vectors in general, is warranted such that means of rational-designing NA vectors can be established. To this end, we adopted N, N'-didodecyl-N, N, N', N'-tetramethyl-N, N'-hexanediyl-di-ammonium dibromide (*p*H unresponsive, herein designated as 12-6-12) and 1,9-bis(dodecyl)-1,1,9,9-tetramethyl-5-imino-1,9-nonanediammonium dibromide (*p*H responsive, herein designated as *p*HC12) from Ref. [10], as well as lipid unilamellar vesicles (LUVs) mimicking the lipid composition of endosomes and lysosomes, and employed UV, fluorescence spectroscopy, and small-angle neutron scattering (SANS) to scrutinize the complexation between DNA and the GSs and the GSs' interactions with the LUVs at varied *p*Hs. Findings from the investigation led to the proposition of an experimentally supported mechanism, which explains the high delivery efficacy of *p*HC12 in particular and of *p*H-responsive NA vectors in general.

II. EXPERIMENT

A. Materials

Chemicals, *N,N*-dimethyldodecylamine (cat. No. D0002, TCI), 1,6-dibromohexane (cat. No. A13417, Alfa Aesar), 1-bromododecane (cat. No. 803268, Merck), 1-bromododecane-d25 (cat. No. DLM-1980-1, Cambridge Isotope Laboratories), 3,3′-iminobis(*N*, *N*-dimethylpropylamine) (cat. No. 348554, Sigma-Aldrich), *N,N,N′,N′*-tetramethyl-1,6-hexanediamine (cat. No. 105139, Sigma-Aldrich), ethanol (cat. No. 8006-05, J. T. Baker), acetone (cat. No. 9006-03, J. T. Baker), ethidium bromide (EtBr, cat. No. E1510, Sigma-Aldrich) and sodium dodecyl sulfate (SDS, cat. No. 75746, Sigma-Aldrich), were used as received. Salmon sperm DNA (cat. No. 15632011) and lipids, dioleoylphosphati-dylcholine (DOPC, cat. No. 850375C), dioleoylphosphatidylethanolamine (DOPE, cat. No. 850725C), dioleoylphosphatidylserine (DOPS, cat. No. 840035C) and cholesterol (Chol, cat. No. 700000P), were purchased from Thermo Fisher Scientific and Avanti Polar Lipids, respectively, and also used without further treatment.

B. Gemini surfactant syntheses

Syntheses of the cationic gemini surfactants (GSs) followed the protocols established elsewhere [10,22]. To synthesize the *p*H-unresponsive 12-6-12 (i.e., N, N'-didodecyl-N, N, N', N'-tetramethyl-N, N'-hexanediyl-di-ammonium dibromide), *N*, *N*-dimethyldodecylamine in excess was mixed with 1,6-dibromohexane in ethanol. The mixed reagents reacted under reflux for 48 h. After ethanol removal, the product underwent several rounds of recrystallization from a mixture of acetone and methanol in the 3:1 (v/v) ratio to recover the surfactant, which was then subjected to overnight drying under vacuum. Similar steps were taken for the synthesis of the *p*H-responsive *p*HC12 (i.e., 1,9-bis(dodecyl)-1,1,9,9-tetramethyl-5-imino-1,9-nonanediammonium dibromide). Here, 1-bromododecane in excess was mixed with 3,3′-iminobis(*N*, *N*-dimethylpropylamine) in ethanol. The reaction proceeded under reflux for 48 h, and purification of the product was carried out via several rounds of recrystallization from a mixture of acetone and water in the 5:1 (v/v) ratio. The chains-deuterated version of the two GSs was synthesized following similar protocols. To synthesize chains-deuterated 12-6-12 (d12-6-12), 1-bromododecane-d25 in excess was mixed with *N,N,N′,N′*-tetramethyl-1,6-hexanediamine; for the synthesis of chains-deuterated *p*HC12 (dpHC12), 1-bromododecane-d25 in excess reacted with 3,3′-iminobis(*N*, *N*-dimethylpropylamine). The chemical identities of the products were verified with ^{1}H NMR, ^{13}C NMR, mass spectrometry, and critical micellar concentration determination (see the Supplemental Material [23]).

C. Preparation of DNA-gemini surfactant complexes and large unilamellar vesicles

Salmon sperm DNA and GSs were separately prepared at desired *p*Hs in the Britton-Robinson buffer, which is an equimolar (40 mM) mixture of boric acid, acetic acid, and phosphoric acid and *p*H-adjusted with sodium hydroxide to cover *p*Hs from 4 to 7. The DNA and GS solutions were mixed in varied molar ratios and incubated at 4 °C overnight to form DNA-GS complexes. In preparing large unilamellar vesicles (LUVs), lipids in the molar ratio, DOPC : DOPE : DOPS : Chol = 40 : 16.7 : 10 : 33.3, were used to mimic endosomal and lysosomal membranes. The lipids were mixed in chloroform and dried by argon gas, followed by 2-h vacuum incubation. Dried lipids were dispersed in the Britton-Robinson buffer at desired *p*Hs. The dispersions were homogenized via five freeze-thaw cycles, with each cycle interspersed by vortex. LUVs were produced by extruding the dispersions through 400-nm orifices on a polycarbonate membrane for >30 cycles. Dynamic light scattering revealed the LUVs to be of 150–250 nm in diameter and with low polydispersity; the diameters are within the common size range of endosomes [24].

D. UV and fluorescence spectroscopy

UV absorption was employed to assess the extent of DNA-GS complexation and binding competition between the complexes and the anionic surfactant, SDS. DNA absorbs UV at 260 nm when dissolved in solutions. Complexation results in DNA's sequestration and decreases UV absorbance (Abs) at this wavelength, while depriving DNA of GSs, as a result of the binding competition with SDS, recovers the UV Abs. The UV spectra were collected at 200–400 nm and fitted against Gaussian and linear functions to account for absorption by DNA and GSs and background. UV Abs of DNA was determined via $\text{Abs} = \ln(I_0/I)$, where I_0 and I are intensities of incident and transmitted UV, respectively. In addition, the complexation of DNA and *p*HC12 was also visualized with atomic force microscopy to confirm formation of the complexes (Fig. S5 [23]).

Binding competition between DNA-GS complexes and the negatively charged LUVs was assessed with fluorescence spectroscopy. Upon being stripped of GSs by LUVs, part of the DNA become accessible to the fluorescent tag, EtBr. Since binding to DNA enhances EtBr fluorescence, the fluorescence intensity reflects the extent to which the complexes

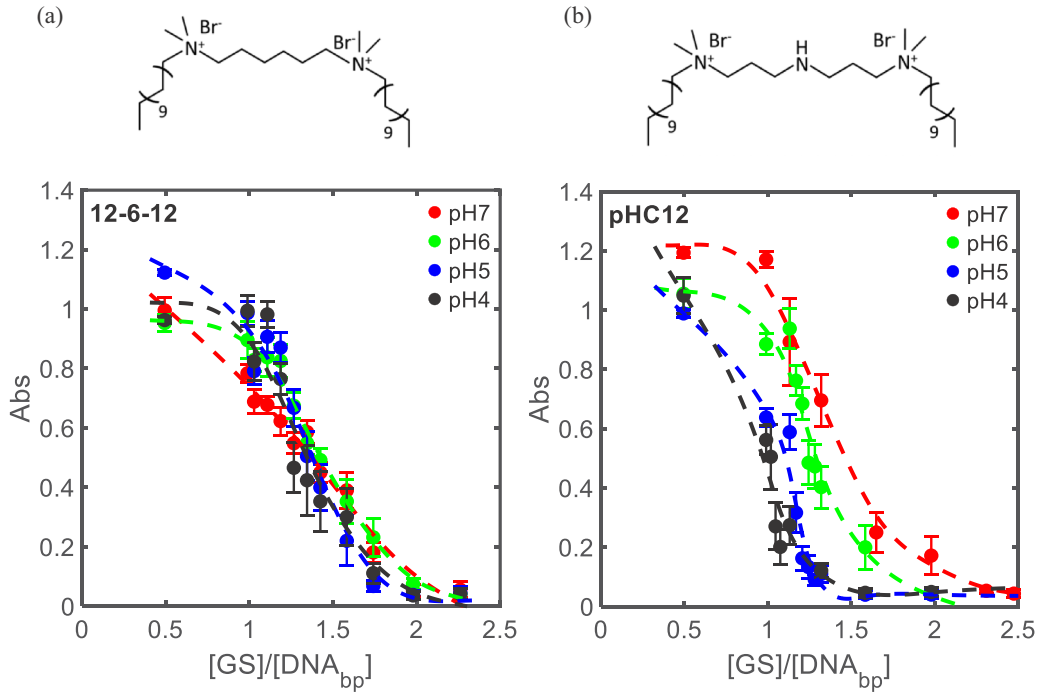

FIG. 1. UV absorption assay for DNA complexation with (a) 12-6-12 or (b) *p*HC12 at varied *p*Hs. Reduction in Abs reflects complexation between DNA and GSs. Efficient vectors are expected to reach large Abs reduction with low vector-to-DNA molar ratios. Dashed lines are to guide the eyes. Chemical structures of the GSs are also shown. Data are expressed as mean ± S.D. and were collected from at least three independently prepared samples.

are dissembled and thus their stability. EtBr was excited at 511 nm and emitted at 590 nm. The measured fluorescence was used to determine the concentration of the DNA base pairs, [DNA_{bp}], which is free of GS, via the relation determined from the calibration curve, $I_f = 21925 \times [DNA_{bp}] + 73$, where I_f is the fluorescence intensity. The proportion of the GS-free base pairs was thus determined as the ratio of [DNA_{bp}] measured before and after the addition to DNA-GS complexes of LUVs. Since the intensity of EtBr fluorescence is essentially unresponsive to acidification [25], any change in the fluorescence intensity is not expected to arise from *p*H variations.

E. Small-angle neutron scattering

Small-angle neutron scattering (SANS) was carried out to investigate the conformational changes of endosome- and lysosome-mimicking LUVs upon their interactions with the GSs. By exploiting differential neutron scattering powers of isotopes, we could exclusively collect the scattering signals from the lipids while leaving the scattering signals from the GSs to be blended with that from the solvent. This was enabled by preparing the mixtures of the LUVs (prepared as described above) and the GSs in the Britton-Robinson buffer made of D_2O:H_2O = 4:1 (v/v). Meanwhile, the chains-deuterated GSs (dGSs), d12-6-12 and dpHC12, whose chains were fully deuterated, were used. In this setting, coherent neutron scattering length density of water matched that of the dGSs such that their scattering contributions were blended and the contribution from the lipids was brought out. For the GS-free LUV samples, the buffer was made of 100% D_2O. The SANS data were collected at the BL15 TAIKAN instrument of the Japan Proton Accelerator Research Complex (J-PARC) and EQ-SANS of Oak Ridge National Laboratory. The SANS data from the samples loaded in the standard banjo cells of 1 mm path length were collected at 25°C with position-sensitive detectors and azimuthally averaged to convert the 2D scattering images to 1D scattering profiles of the scattering intensity $I(|\vec{Q}|)$ against $|\vec{Q}| = 4\pi \sin\theta/\lambda$, where 2θ is the scattering angle and λ is the wavelength of incident neutron. The scattering profiles were corrected for detector sensitivity and background and were fitted against various models of lipid self-assemblies in the SASVIEW program; the size distributions of the lipid assemblies were described with lognormal functions, as recommended by the program.

III. RESULTS AND DISCUSSION

A. *p*HC12 is superior in compacting DNA at low *p*Hs than at high *p*Hs

A primary use of a NA vector is to compact NAs by forming complexes with them. Via electrostatic attraction, the cationic GSs, 12-6-12 and pHC12 (see Fig. 1 for chemical structures), can drape over the DNA surface, screen negative charges of its phosphates, reduce its intramolecular electrostatic repulsion, and thereby compact it. The DNA complexation efficacy of the GSs can be assessed with UV absorption. DNA absorbs UV at 260 nm when dispersed in solutions. Complexation would sequester DNA and decrease UV absorbance (Abs) [26,27]. Here, UV absorption was measured at varied *p*Hs and in varied GS-to-DNA molar ratios,

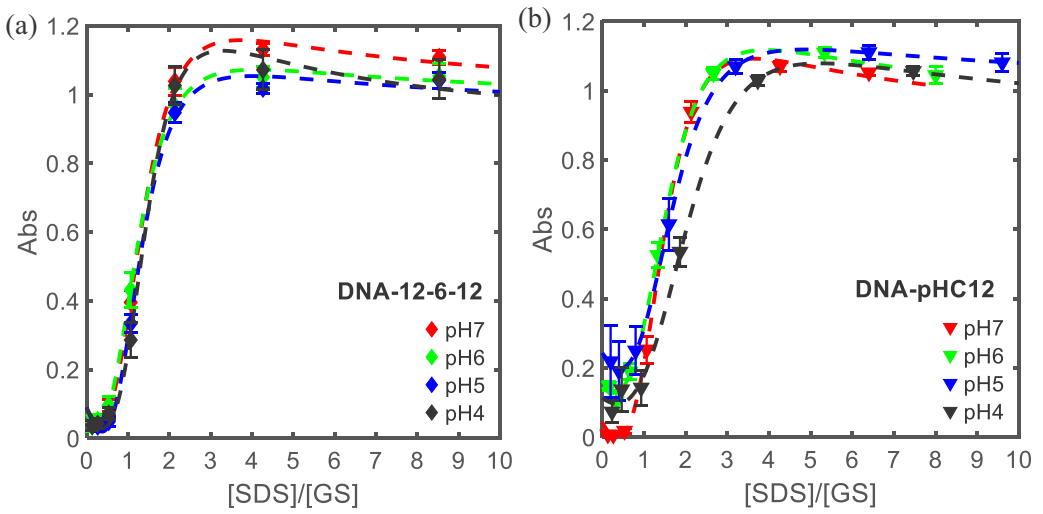

FIG. 2. UV absorption assay for binding competition between the anionic surfactant SDS and (a) DNA-12-6-12 or (b) DNA-*p*HC12 complexes at varied *p*Hs. The competition can result in the GS binding to SDS and re-disperse DNA to make it UV detectable. Stable complexes are expected to require high SDS-to-GS molar ratios to be destabilized and reach certain Abs elevation. Dashed lines are to guide the eyes. The GS-to-DNA_{bp} molar ratios were (a) ∼2.3 mol/mol for all *p*Hs; and (b) ∼2.4 mol/mol, ∼2.0 mol/mol, ∼1.5 mol/mol, and ∼1.3 mol/mol for $pH = 7$, 6, 5, and 4, respectively. Data are expressed as mean ± S.D. and were collected from at least three independently prepared samples.

with the concentration of the DNA base pairs, $[DNA_{bp}]$, fixed at 47.4 μM.

While both the GSs demonstrated the capability to complex with and compact DNA at all the *p*Hs, *p*HC12 was obviously distinct from 12-6-12 when it comes to complexation at high acidity (Fig. 1). At low acidity, there is no conspicuous difference between the two GSs in the GS-to-DNA_{bp} molar ratio minimally required to achieve Abs ≈ 0, presumably the point of saturated complexation. However, as acidity rose, this minimal molar ratio considerably dropped for *p*HC12 whereas that ratio for 12-6-12 was essentially unchanged (Fig. 1). At $pH = 4$, the amount of *p*HC12 required for Abs ≈0 was reduced to the extent that *p*HC12 could saturate the complexation with only half of the amount needed for 12-6-12. The *p*H-responsiveness of the complexation for *p*HC12 presumably arises from the low pK_a ($pK_a \approx 5$) of *p*HC12's amine group [10], which makes it more positively charged at low *p*Hs.

This finding has implications for endosomal escape of the DNA-GS complexes. When used in transfection, the complexes are prepared at neutral acidity and contain specific amounts of 12-6-12 or *p*HC12. Upon entering cells via endocytosis, the complexes reside in an increasingly acidic environment [18]. Since a smaller amount of *p*HC12 is required to maintain intactness of the complexes at high acidity (Fig. 1), the *p*HC12 molecules initially contained in the complexes can become excessive. These extra *p*HC12 molecules might be shed to the endosome lumen, structurally perturb endosomal and lysosomal membranes, and in turn assist endosomal escape of the complexes. We will return to this speculation in a following section. On the other hand, elevated acidity does not reduce the 12-6-12 amount required to maintain complex integrity. Therefore, it is likely that no significant amount of 12-6-12 is freed from the complexes upon acidification inside endosomes and lysosomes.

B. DNA-*p*HC12 complexes exhibit higher stability at all *p*Hs

Stability of the DNA-GS complexes was assessed with a UV-based binding competition assay. Here, the complexes were prepared so that their GS-to-DNA_{bp} molar ratios were close to the minimal ratios required to saturate the complexation, which were ∼2.3 mol/mol for 12-6-12 at all *p*Hs and ∼2.4, ∼2.0, ∼1.5, and ∼1.3 mol/mol for *p*HC12 at $pH = 7$, 6, 5, and 4, respectively. An anionic surfactant, sodium dodecyl sulfate (SDS), was added to the DNA-GS complex solutions and competed with DNA for binding with the GSs. (The final $[DNA_{bp}]$ was 35.6 μM after the SDS addition.) GS retrieving by SDS can disrupt the complexes and redisperse DNA in the solution. Since the redispersion elevates Abs, how readily Abs rises with [SDS] should reflect the stability of the complexes.

For both of the GSs, Abs increased sharply with [SDS] for low SDS-to-GS molar ratios but reached a plateau of Abs ≈ 1 when the molar ratio surpassed certain values (Fig. 2). The molar ratios for the onset of the plateau presumably reflect stability of the complexes, as complexes of higher stability resist the SDS-induced disruption more strongly and require a higher [SDS] to reach the plateau. For 12-6-12, the plateau was reached when the SDS-to-GS molar ratio surpassed ∼2 mol/mol, regardless of *p*H. On the other hand, the plateau-onset molar ratio for *p*HC12 was slightly greater than that for 12-6-12 in general and showed clear *p*H dependence, with higher acidity leading to higher plateau-onset molar ratios. Hence, DNA-*p*HC12 complexes were not only more stable but also more acid-proof (or even "acid-hardened") than their 12-6-12 counterpart. This is particularly striking when one recalls that the DNA-*p*HC12 complexes examined here for $pH = 4$ contained fewer GS molecules than the DNA-*p*HC12 complexes at the other *p*Hs and the DNA-12-6-12 complexes at any *p*H. Accordingly, DNA-*p*HC12 complexes used in transfection might become more stable upon acidification,

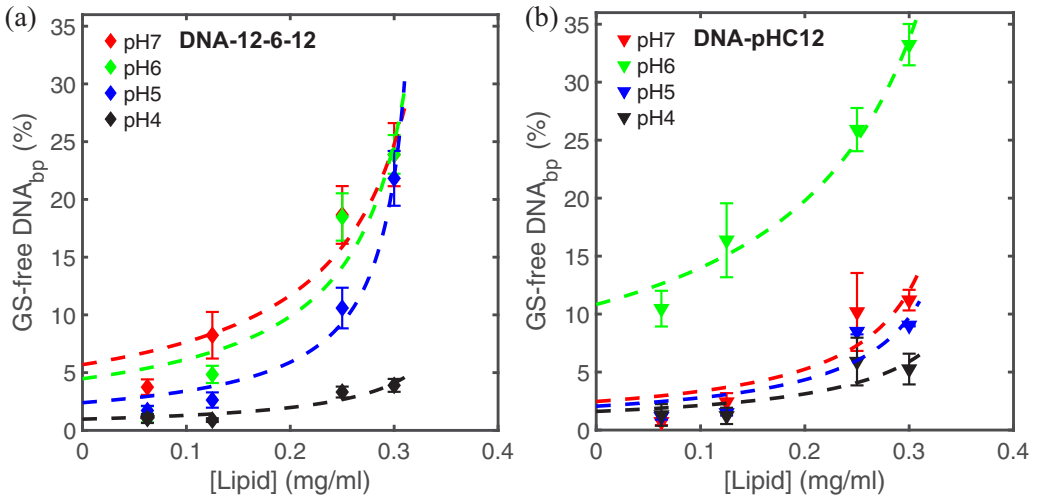

FIG. 3. Fluorescence assay for binding competition between endosome- and lysosome-mimicking LUVs and (a) DNA-12-6-12 or (b) DNA-*p*HC12 complexes at varied *p*Hs. The competition can strip DNA base pairs of the GSs and allow the fluorescence tag, EtBr, to bind to the GS-free base pairs, which enhances EtBr fluorescence. Stable complexes are expected to have low proportions of GS-free base pairs at a given lipid concentration. Dashed lines are fits against a mass-balance-based equation. Data are expressed as mean ± S.D. and were collected from at least three independently prepared samples.

even as acidification can prod the complexes to shed the excessive *p*HC12 molecules to the endosome lumen (see the previous section).

Setting aside the artificial binding competition with SDS, DNA in DNA-GS complexes may in reality face binding competition with endosomal and lysosomal membranes when the complexes are engulfed in endosomes and lysosomes. Endosomal and lysosomal membranes contain a significant amount of the acidic phospholipid, phosphatidylserine [28], and are negatively charged. Upon competition, the complexes may be partially deprived of their GS molecules and consequently extend their DNA molecules and expose them to the degradative lysosomal enzymes. Stability against this competition can therefore be crucial to effective intracellular delivery of NAs. Here, we employed a fluorescence assay to assess stability of the DNA-GS complexes (in the same GS-to-DNA$_{bp}$ molar ratios as those for the SDS assay) against binding competition with endosomal and lysosomal membranes. LUVs of ∼200 nm and composed of the lipids, DOPC (dioleoylphosphatidylcholine), DOPE (dioleoylphosphatidylethanolamine), DOPS (dioleoylphosphatidylserine), and Chol (cholesterol) in the molar ratio of 40:16.7:10:33.3, were used as a model of endosomal and lysosomal membranes, and the lipid concentrations in the same order of magnitude as those experienced by GSs inside an endosome were employed. The fluorescent tag, ethidium bromide (EtBr), which binds to DNA when DNA is exposed to the solution, was employed. (The final [DNA$_{bp}$] was 47.4 μM after the LUV and EtBr addition.) Since binding to DNA enhances EtBr fluorescence, the fluorescence intensity should reflect the extent of the competition-induced solvent exposure of DNA and thus stability of the complexes.

The proportions of the DNA base pairs free of GSs were derived from the fluorescence intensities (see Sec. II for details) for varied [Lipid] (Fig. 3). The [Lipid] dependence of the proportion can be fitted with an equation derived from a mass-balance analysis for the competitive binding and solved according to Refs. [29,30] (see the Supplemental Material [23] for more details); how readily the proportion rose with [Lipid] might reflect stability of the complexes, with a steeper rise indicating weaker stability. Unlike the SDS assays presented above, both DNA-12-6-12 and DNA-*p*HC12 demonstrated clear dependence on acidity when it comes to stability against binding competition with LUVs, albeit the dependence followed distinct trends for the two complex types. For DNA-12-6-12 at a given lipid concentration, say [Lipid] = 0.3 mg/ml, the proportion of the GS-free DNA base pairs was slightly lower at *p*H = 5–6 and greatly lower at *p*H = 4, compared with the proportion at *p*H = 7. These likely reflected its improved stability in acidic environments or protonation of the anionic DOPS, particularly at *p*H = 4. For DNA-*p*HC12, the proportion of the GS-free DNA base pairs at *p*H = 7 was significantly lower than that of DNA-12-6-12 to begin with. Higher acidity further decreased the proportion for DNA-*p*HC12, except for *p*H = 6. In comparison, the proportions of the GS-free DNA base pairs are comparable for DNA-*p*HC12 and DNA-12-6-12 at *p*H = 4 and 6. However, at *p*H = 5 and 7, the proportions for DNA-*p*HC12 are considerably lower than that for DNA-12-6-12. Accordingly, DNA-*p*HC12 appears to display stronger stability against binding competition with endosomal and lysosomal membranes than DNA-12-6-12. This inference holds true even when protonation of DOPS at *p*H = 4 is taken into consideration, which should have occurred in both cases, if it did occur. This difference might make or break intracellular NA delivery. In endocytosis, acidity inside endosomes turns from *p*H = 7.4, through *p*H = 6 and 5 at the early and late endosome stages, respectively, to *p*H = 4.5 upon their maturation into lysosomes. During this acidity variation, higher stability against binding competition with endosomal and lysosomal membranes at *p*H = 5 might allow DNA-*p*HC12 complexes to better protect DNA from enzymatic degradation than their 12-6-12 counterpart.

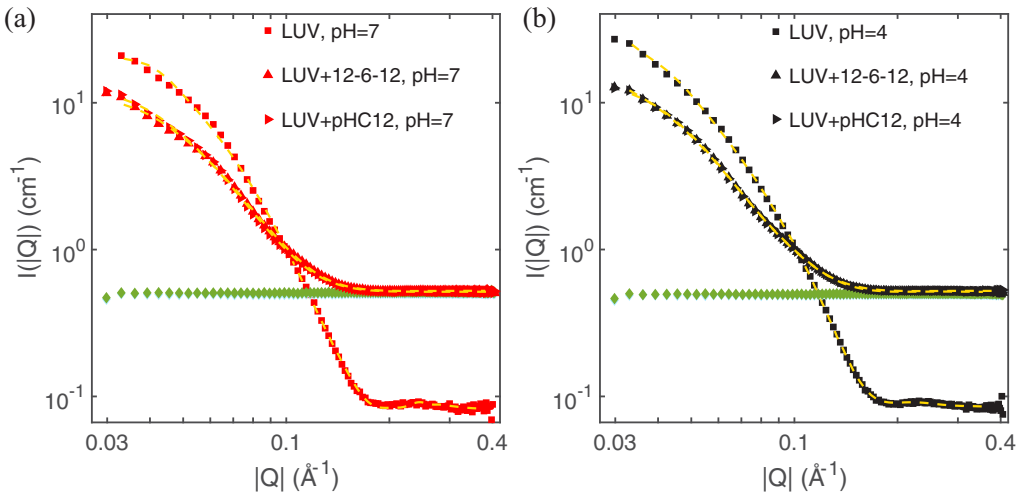

FIG. 4. SANS profiles of absolute scattering intensity I against momentum transfer $|\vec{Q}|$ for endosome- and lysosome-mimicking LUVs with or without adding the dGSs at (a) $p\mathrm{H} = 7$ and (b) $p\mathrm{H} = 4$. Dashed lines are fittings against the structural models of hollow vesicle (for GS-free samples) and micelle (for GS-containing samples). The scattering data for the dGSs alone (diamonds) confirm the matching of coherence scattering length densities of the dGSs and the buffer.

C. Both *p*HC12 and 12-6-12 structurally perturb LUVs

It is known from previous sections that DNA-*p*HC12 can have excessive GS molecules upon acidification and that binding competition between DNA and endosomal and lysosomal membranes can strip GSs from both DNA-*p*HC12 and DNA-12-6-12. These breakaway GS molecules may structurally perturb the membranes. Here, we employed SANS in combination with the contrast-matching scheme to explore the possible perturbation by the GSs to endosome- and lysosome-mimicking LUVs. The approach, based on differential neutron scattering powers of isotopes, was implemented by deuterating the hydrocarbon chains of the GSs (dGSs) and mixing H_2O and D_2O in preparing the buffer where the samples were dispersed. H_2O and D_2O were mixed in the 4:1 (v/v) ratio such that the scattering powers of the dGSs matched that of water. This matching allowed us to deduct the SANS signals of the dGSs and water from that of an entire sample. Consequently, only the SANS signal of the lipids was left for the ensuing processing. dGS-induced perturbations to the LUVs could thereby be unambiguously probed.

A comparison for the LUVs with and without adding the dGSs reveals that both 12-6-12 and *p*HC12, in the dGS-to-lipid molar ratio of ∼1:50, could drastically change the SANS profile (i.e., the plot of scattering intensity I against momentum transfer $|\vec{Q}|$, where $|\vec{Q}| = 4\pi \sin\theta/\lambda$ with 2θ being the scattering angle and λ the wavelength of incident neutrons) of the lipids (Fig. 4). The change persisted when acidity was elevated to $p\mathrm{H} = 4$ for both of the GSs, despite their differential responsiveness to acidification. This change in SANS profile is expected to arise from structural changes to the LUVs upon their interactions with the dGSs. A detailed analysis involving fitting the profiles against the models for the lipid self-assembled structures was also carried out. In the absence of the dGSs, the SANS profiles at $p\mathrm{H} = 7$ and 4 can be fitted with the unilamellar vesicle model, giving a radius of ∼200 nm, which is larger than but still consistent with that from the dynamic light scattering measurement (see Sec. II). At both $p\mathrm{H} = 7$ and 4, adding the dGSs gave rise to the SANS profiles of the lipids incompatible with the unilamellar vesicle model. Instead, these profiles can be described with the model for micelles in the radii of 2–3 nm (Fig. 4). The obtained fitting parameters are summarized in Table I. Readers are cautioned that structural changes involving other lipid self-assemblies cannot be excluded even though the result of the fittings is suggestive of a LUV-to-micelle transformation for the lipids after the LUVs interacted with the dGSs. Nevertheless, it is certain that the dGSs can structurally perturb the LUVs.

D. Acidification-induced excess of *p*HC12 and high complex stability may contribute to the high transfection efficacy of *p*HC12

Based on the observations above, a mechanism potentially underlying the high transfection efficacy of *p*HC12 is envisioned. Upon acidification during endocytosis, the initial amount of *p*HC12 in the complexes would become increasingly excessive since fewer *p*HC12 molecules are required to complex with DNA. The excessive *p*HC12 molecules may be shed from the complexes (the shedding may be enhanced by binding competition between DNA and endosomal and lysosomal membranes) and set free to structurally perturb endosomal and lysosomal membranes (possibly transforming part of the membranes from bilayers to micelles). This structural perturbation in turn assists the escape from endosomes and lysosomes of the complexes, before they are enzymatically degraded, and thus facilitates transfection. Besides, DNA-*p*HC12 complexes may display high stability against binding competition with endosomal and lysosomal membranes and remain protective to the DNA cargos even after shedding excessive *p*HC12 molecules. The GS excess and high stability are thus expected to underlie the high transfection efficacy of *p*HC12. On the other hand, the amount of 12-6-12 needed for complexing with DNA barely changes

TABLE I. Structural dimensions of lipid self-assemblies extracted from the fitting parameters of SANS.

	Lipid	Lipid + 12-6-12	Lipid + *p*HC12
SANS fitting model	hollow vesicle	core-shell micelle	core-shell micelle
*p*H = 7			
Radius (Å)[a]	2046.4	27.8	27.2
Headgroup layer thickness (Å)	8.4	13.7	13.1
Chain layer thickness[a] (Å)	25.0	28.2	28.2
Background (1/cm)	0.08	0.52	0.51
Lognormal distribution width	0.0004	0.5	0.5
*p*H = 4			
Radius (Å)[a]	1514.5	22.2	23.8
Headgroup layer thickness (Å)	9.9	16.9	14.9
Chain layer thickness[a] (Å)	22.9	10.6	17.8
Background (1/cm)	0.08	0.51	0.51
Lognormal distribution width	0.0001	1.0	0.7

[a]For micelles, the radius is the sum of the headgroup layer thickness and half a chain layer thickness.

with acidity. Therefore, DNA-12-6-12 complexes may not be able to cause strong perturbations to endosomal and lysosomal membranes during endosome maturation. Moreover, the complexes are less stable against binding competition with the membranes. The few 12-6-12 molecules deprived from the complexes due to the lower stability may still minimally perturb the membranes but at the expense of complex integrity.

Perturbing endosomal and lysosomal membranes by free vector molecules is not unique to *p*HC12. Similar observations were reported for the workhorse polymer vector polyethylenimine (PEI) [21]. When prepared in excess, PEI molecules bound to and free from DNA were simultaneously present in the complex preparations. By preventing DNA-PEI complexes from being entrapped in endosomes, free PEI enhanced transfection efficacy by up to 10^3 times, compared to the preparations without excessive PEI. The entrapment prevention was considered to arise from the destabilization of endosomal membranes and disruption of the endosome-lysosome fusion by free PEI molecules. It was also found that proton sponge is not a dominant mechanism responsible for the high transfection efficacy of PEI, since chemically inhibiting endosomal proton pumps, the proper functioning of which is critical to the proton sponge (see Sec. I), only slightly depressed transfection efficacy. Our findings here are largely consistent with the PEI observations, only that the free vector molecules here were released upon acidification, instead of being preexistent in the preparations. This is actually of benefit since it eases the requirement for preserving and codelivering free vector molecules. This requirement can be practically challenging for *in vivo* delivery of NA, as free vector molecules might induce strong immune responses and be sequestered from the complexes long before they reach targets.

IV. CONCLUSION

Employing UV and fluorescence spectroscopy, we quantified the capabilities to compact DNA and withstand binding competition for the GSs, 12-6-12 and *p*HC12, in their capacity as NA vectors. *p*H-responsive *p*HC12 displayed better DNA complexation efficacy in acidic than in neutral environments, manifested as requiring fewer *p*HC12 molecules to reach a given extent of DNA complexation, whereas 12-6-12 was unresponsive to acidification in this regard. On the aspect of withstanding binding competition, DNA-*p*HC12 complexes were more stable, and became even more so upon acidification, than DNA-12-6-12 complexes against binding competition with SDS and endosome- and lysosome-mimicking LUVs. Via the contrast-matching SANS technique, we also found that both free 12-6-12 and *p*HC12 could structurally perturb endosome- and lysosome-mimicking LUVs. Taken together, these findings suggest a potential mechanism accounting for the observation reported in Ref. [10] where the *p*H-responsive GSs achieved higher NA delivery efficacy than their *p*H-unresponsive counterparts: The *p*H-responsive GS molecules that become excessive to the complexes and, without sacrificing complex integrity, are shed upon acidification during endocytosis structurally perturb endosomal and lysosomal membranes and thereby facilitate endosomal escape of the complexes. Besides, enhanced stability of the *p*H-responsive complexes upon acidification is also of benefit to NA delivery. Both of the acidification-induced vector excess and stability enhancement are not expected for the *p*H-unresponsive GSs, which possibly results in their lower NA efficacy. A design principle for NA vectors might emerge from this mechanism: The more the *p*H-responsive functional groups present in a vector molecule, the higher the delivery efficacy of a vector. This principle deserves further scrutiny.

ACKNOWLEDGMENTS

This study was supported by the Ministry of Science and Technology, Taiwan (Grant No. MOST 110-2221-E-008-007) and by National Central University. Work at J-PARC was carried out under the user program (Proposal No. 2018B0252), and work at ORNL's Spallation Neutron Source was sponsored by the Scientific User Facilities Division, Office of Basic Energy Sciences, U.S. Department of Energy.

[1] J. A. Kulkarni, D. Witzigmann, S. B. Thomson, S. Chen, B. R. Leavitt, P. R. Cullis, and R. van der Meel, The current landscape of nucleic acid therapeutics, Nat. Nanotechnol. **16**, 630 (2021).

[2] T. C. Roberts, R. Langer, and M. J. A. Wood, Advances in oligonucleotide drug delivery, Nat. Rev. Drug Discov. **19**, 673 (2020).

[3] M. Qiu, Z. Glass, J. Chen, M. Haas, X. Jin, X. Zhao, X. Rui, Z. Ye, Y. Li, F. Zhang, and Q. Xu, Lipid nanoparticle-mediated codelivery of Cas9 mrna and single-guide RNA achieves liver-specific in vivo genome editing of Angptl3, Proc. Natl. Acad. Sci. USA **118**, e2020401118 (2021).

[4] C.-F. Xu, G.-J. Chen, Y.-L. Luo, Y. Zhang, G. Zhao, Z.-D. Lu, A. Czarna, Z. Gu, and J. Wang, Rational designs of in vivo crispr-cas delivery systems, Adv. Drug. Deliv. Rev. **168**, 3 (2021).

[5] M. D. Shin, S. Shukla, Y. H. Chung, V. Beiss, S. K. Chan, O. A. Ortega-Rivera, D. M. Wirth, A. Chen, M. Sack, J. K. Pokorski, and N. F. Steinmetz, COVID-19 vaccine development and a potential nanomaterial path forward., Nat. Nanotechnol. **15**, 646 (2020).

[6] H. J. Vaughan, J. J. Green, and S. Y. Tzeng, Cancer-Targeting nanoparticles for combinatorial nucleic acid delivery, Adv. Mater. **32**, 1901081 (2020).

[7] O. S. Fenton, K. N. Olafson, P. S. Pillai, M. J. Mitchell, and R. Langer, Advances in biomaterials for drug delivery, Adv. Mater. **30**, 1705328 (2018).

[8] D. Vercauteren, J. Rejman, T. F. Martens, J. Demeester, S. C. De Smedt, and K. Braeckmans, On the cellular processing of non-viral nanomedicines for nucleic acid delivery: Mechanisms and methods, J. Controlled Release **161**, 566 (2012).

[9] M. Gharagozloo, A. Rafiee, D. W. Chen, and M. Foldvari, a flow cytometric approach to study the mechanism of gene delivery to cells by gemini-lipid nanoparticles: An implication for cell membrane nanoporation, J. Nanobiotechnology **13**, 62 (2015).

[10] M. Donkuru, S. D. Wettig, R. E. Verrall, I. Badea, and M. Foldvari, Designing pH-sensitive gemini nanoparticles for non-viral gene delivery into keratinocytes, J. Mater. Chem. **22**, 6232 (2012).

[11] N. Kongkatigumjorn, S. A. Smith, M. Chen, K. Fang, S. Yang, E. R. Gillies, A. P. R. Johnston, and G. K. Such, Controlling endosomal escape using pH-Responsive nanoparticles with tunable disassembly, ACS Appl. Nano Mater. **1**, 3164 (2018).

[12] K. Sakamoto, M. Akishiba, T. Iwata, K. Murata, S. Mizuno, K. Kawano, M. Imanishi, F. Sugiyama, and S. Futaki, Optimizing charge switching in membrane lytic peptides for endosomal release of biomacromolecules, Angew. Chem., Int. Ed. Engl. **59**, 19990 (2020).

[13] D. Habrant, P. Peuziat, T. Colombani, L. Dallet, J. Gehin, E. Goudeau, B. Evrard, O. Lambert, T. Haudebourg, and B. Pitard, Design of ionizable lipids to overcome the limiting step of endosomal Escape: Application in the intracellular delivery of mRNA, DNA, and sirna, J. Med. Chem. **59**, 3046 (2016).

[14] D. Pei and M. Buyanova, Overcoming endosomal entrapment in drug delivery, Bioconjug. Chem. **30**, 273 (2019).

[15] S. A. Smith, L. I. Selby, A. P. R. Johnston, and G. K. Such, The endosomal escape of Nanoparticles: Toward more efficient cellular delivery, Bioconjug. Chem. **30**, 263 (2019).

[16] X. A. Wu, C. H. J. Choi, C. Zhang, L. Hao, and C. A. Mirkin, Intracellular fate of spherical nucleic acid nanoparticle conjugates, J. Am. Chem. Soc. **136**, 7726 (2014).

[17] J. Gilleron, W. Querbes, A. Zeigerer, A. Borodovsky, G. Marsico, U. Schubert, K. Manygoats, S. Seifert, C. Andree, M. Stöter, H. Epstein-Barash, L. Zhang, V. Koteliansky, K. Fitzgerald, E. Fava, M. Bickle, Y. Kalaidzidis, A. Akinc, M. Maier, and M. Zerial, Image-based analysis of lipid nanoparticle-mediated sirna delivery, intracellular trafficking and endosomal escape, Nat. Biotechnol. **31**, 638 (2013).

[18] I. Mellman, R. Fuchs, and A. Helenius, Acidification of the endocytic and exocytic pathways, Annu. Rev. Biochem. **55**, 663 (1986).

[19] L. M. P. Vermeulen, S. C. De Smedt, K. Remaut, and K. Braeckmans, The proton sponge hypothesis: Fable or fact? Eur. J. Pharm. Biopharm. **129**, 184 (2018).

[20] T. C. B. Klauber, R. V. Søndergaard, R. R. Sawant, V. P. Torchilin, and T. L. Andresen, Elucidating the role of free polycations in gene knockdown by sirna polyplexes, Acta Biomater. **35**, 248 (2016).

[21] Y. Yue, F. Jin, R. Deng, J. Cai, Z. Dai, M. C. M. Lin, H.-F. Kung, M. A. Mattebjerg, T. L. Andresen, and C. Wu, Revisit complexation between DNA and polyethylenimine–effect of length of free polycationic chains on gene transfection, J. Controlled Release **152**, 143 (2011).

[22] A. R. Tehrani Baghaa, H. Bahrami, B. Movassagh, M. Arami, and F. M. Menger, Interactions of gemini cationic surfactants with anionic azo dyes and their inhibited effects on dyeability of cotton fabric, Dyes Pigm. **72**, 331 (2007).

[23] See Supplemental Material at http://link.aps.org/supplemental/10.1103/PhysRevE.106.034408 for the spectra of ^{1}H NMR, ^{13}C NMR, and mass spectrometry and critical micellar concentration of the gemini surfactants.

[24] L. M. P. Vermeulen, T. Brans, S. K. Samal, P. Dubruel, J. Demeester, S. C. De Smedt, K. Remaut, and K. Braeckmans, Endosomal size and membrane leakiness influence proton sponge-based rupture of endosomal vesicles, ACS Nano **12**, 2332 (2018).

[25] P. O. Vardevanyan, A. P. Antonyan, M. A. Parsadanyan, H. G. Davtyan, and A. T. Karapetyan, The binding of ethidium bromide with DNA: Interaction with single- and double-stranded structures, Exp. Mol. Med. **35**, 527 (2003).

[26] O. Le Bihan, R. Chèvre, S. Mornet, B. Garnier, B. Pitard, and O. Lambert, Probing the in vitro mechanism of action of cationic lipid/DNA lipoplexes at a nanometric scale, Nuc. Acids Res. **39**, 1595 (2011).

[27] J. Carlstedt, D. Lundberg, R. S. Dias, and B. Lindman, Condensation and decondensation of DNA by cationic surfactant, spermine, or cationic surfactant-cyclodextrin mixtures: Macroscopic phase behavior, aggregate properties, and dissolution mechanisms, Langmuir **28**, 7976 (2012).

[28] G. van Meer, D. R. Voelker, and G. W. Feigenson, Membrane lipids: Where they are and how they behave, Nat. Rev. Mol. Cell Biol. **9**, 112 (2008).

[29] Z. -X. Wang, An exact mathematical expression for describing competitive binding of two different ligands to a protein molecule, FEBS Lett. **360**, 111 (1995).

[30] M. S. Dietz, S. S. Wehrheim, M.-L. I. E. Harwardt, H. H. Niemann, and M. Heilemann, Competitive binding study revealing the influence of fluorophore labels on biomolecular interactions, Nano Lett. **19**, 8245 (2019).